# Sodium Tantalate Photocatalysts Doped with Metal Cations: Why Are They Active for Water Splitting?

Onishi, Hiroshi

(Citation)
ChemSusChem,12(9):1825-1834

(Issue Date)
2019-05-08

(Resource Type)
journal article

(Version)
Version of Record

ChemPubSoc Europe

DOI: 10.1002/cssc.201802935

CHEMSUSCHEM Minireviews

# Sodium Tantalate Photocatalysts Doped with Metal Cations: Why Are They Active for Water Splitting?

Hiroshi Onishi*[a]

Sodium tantalate ($NaTaO_3$) is the first semiconductor photocatalyst that produces hydrogen–oxygen mixed bubbles in the overall water splitting reaction, when appropriately doped with metal cations. A series of studies are reviewed herein to answer the question of why doping with metal cations raised the quantum efficiency of the reaction. Infrared absorption of band-gap-excited photocatalysts demonstrated that cation doping reduced the electron–hole recombination rate and the steady-state population of charge carriers accordingly increased. In-depth studies are focused on Sr cations incorporated through solid-state, flux, and hydrothermal reactions. The recombination rate was reduced when Ta cations were exchanged with Sr cations. Sodium cations were simultaneously exchanged to balance the cationic and anionic charges with no need for creating oxygen anion vacancies. $NaTaO_3$-$Sr(Sr_{1/3}Ta_{2/3})O_3$ solid solution was formed as a result of the simultaneous doping. In addition to doping at the appropriate sites, the intraparticle distribution of Sr cations played an essential role to reduce the recombination rate. Strontium cations segregated to produce graded composition from the Sr-rich surface to the Sr-poor core. The bottom of the conduction band was raised at the Sr-rich surface and the excited electrons were driven to the Sr-poor core, leaving holes at the surface. However, the graded composition had a dual purpose; the excited electron population increased and its fractional contribution to the surface reaction decreased.

## 1. Introduction

Sodium tantalate ($NaTaO_3$) is the first semiconductor photocatalyst known to produce mixed hydrogen–oxygen bubbles in the absence of any sacrificial reagent. The apparent quantum efficiency, which is defined as the ratio of the number of electrons (or holes) consumed in the reaction to the the number of incident photons into the reaction vessel, exceeded 50% when Kudo and co-workers modified this metal oxide by doping it with La cations and loading NiO cocatalyst. [1,2] The $H_2$ and $O_2$ production rates over these photocatalysts were reported in the unit of mmol per hour, whereas those on previously reported photocatalysts were reported in the unit of μmol per hour. The application to photocatalytic $CO_2$ reduction has also been successfully examined.[3,4]

Inspired by the achievements of Kudo and co-workers, a large number of studies have since been conducted to develop $NaTaO_3$-based photocatalysts that are efficient for artificial photosynthesis, with more than 180 studies, as well as reviews,[5–8] reported to date.[9] Doping with lanthanoid cations,[1] not limited to $La^{3+}$, and alkaline-earth metal cations[10,11] improved the water splitting efficiency (Table 1). These findings suggest that $La^{3+}$ is not unique as a guest cation in improving the efficiency, although it provided the best record in the $NaTaO_3$ host. Sakata and co-workers[12] developed $Ga_2O_3$ photocatalysts that showed an even higher efficiency of 71% when

**Table 1.** The rate of overall water splitting on $NaTaO_3$ doped with metal cations through a solid-state reaction.[a]

| Doping cation | Doping concentration [mol%] | $H_2$ production [mmol $h^{-1}$] | $O_2$ production [mmol $h^{-1}$] | band gap [eV] | NiO cocatalyst loading [wt%] | Ref. |
|---|---|---|---|---|---|---|
| none | - | 1.7 | 0.8 | 4.0 | 0.05 | [10] |
| $La^{3+}$ | 2 | 19.8 | 9.7 | 4.1 | 0.2 | [2] |
| $Ca^{2+}$ | 2 | 4.9 | 2.4 | 4.1 | 0.2 | [10] |
| $Sr^{2+}$ | 2 | 9.5 | 4.7 | 4.1 | 0.2 | [10] |
| $Ba^{2+}$ | 2 | 9.3 | 4.7 | 4.1 | 0.2 | [10] |
| $Pr^{3+}$ | 1 | 5.3 | 2.6 | 4.1 | 0.05 | [1] |
| $Nd^{3+}$ | 1 | 5.2 | 2.5 | 4.1 | 0.05 | [1] |
| $Sm^{3+}$ | 1 | 5.3 | 2.6 | 4.1 | 0.05 | [1] |
| $Gd^{3+}$ | 1 | 4.3 | 2.1 | 4.1 | 0.05 | [1] |
| $Tb^{3+}$ | 1 | 4.3 | 2.2 | 4.1 | 0.05 | [1] |
| $Dy^{3+}$ | 1 | 4.5 | 2.2 | 4.1 | 0.05 | [1] |

[a] Aqueous suspension of the photocatalyst (1 g in refs. [1 and 2], 0.5 g in ref. [10]) was irradiated in an inner irradiation vessel with a 400 W high-pressure Hg lamp. The photocatalysts were prepared by a solid-state reaction.

[a] Dr. H. Onishi
Department of Chemistry, School of Science, Kobe University
Rokko-dai, Nada, Kobe, Hyogo 657-8501 (Japan)
E-mail: oni@kobe-u.ac.jp

The ORCID identification number(s) for the author(s) of this article can be found under:
https://doi.org/10.1002/cssc.201802935.



This publication is part of a Special Issue focusing on "Water Splitting: From Theory to Practice".
Please visit the issue at http://doi.org/10.1002/cssc.v12.9.

 

doped with $Zn^{2+}$. Quite recently, Domen and co-workers[13] pushed water splitting efficiency on $SrTiO_3$ up to 69% by doping with $Al^{3+}$. $NaTaO_3$ is not a unique host to be activated by cation doping. It should be recognized that doping with metal cations offers a common means of increasing water splitting efficiency close to unity.

However, the mechanisms behind the increased efficiency are unknown. Guest metal cations are impurities that introduce defects to the host lattice. Impurities are thought to immobilize band-gap-excited charge carriers and even catalyze electron–hole recombination. The unknown mechanisms, when revealed, can be applied to a broad range of metal oxide photocatalysts including those sensitized to visible light, although the host compounds quoted above require ultraviolet (UV) light to be band-gap-excited. With an ambition to reveal the mechanisms in mind, the author and co-workers have studied cation doping in $NaTaO_3$ photocatalysts to determine why quantum efficiency increases. Their results and interpretations are presented herein, following a brief summary of crystallographic and electronic structures of pristine alkali tantalates.

## 2. Alkali Tantalates

$NaTaO_3$ possesses a perovskite-structured lattice with monovalent Na cations in A sites and pentavalent Ta cations in B sites. Cations and anions are closely packed in a perovskite-structured lattice with limited freedom to occupy interstitial positions. The tolerance factor $t$ is defined by Equation (1):

$$t = \frac{r_A + r_O}{\sqrt{2}(r_B + r_O)} \quad (1)$$

to quantify the degree of packing, with ionic radii of A-site cation, B-site cation, and oxygen anion given as $r_A$, $r_B$, and $r_O$, respectively. When the three hard-sphere ions are in contact, the factor goes to unity. According to the ionic radii listed in ref. [14], $NaTaO_3$ has a factor of 0.97, suggesting finite room left in the lattice. By filling the room, the originally cubic lattice is distorted to be orthorhombic (space group *Pbnm*; $a = 0.548$, $b = 0.552$, $c = 0.779$ nm) at room temperature (Figure 1 a).[15] An orthorhombic cell contains four $NaTaO_3$ units. A cube with sides of 0.389 nm, the volume of which corresponds to one fourth of the orthorhombic cell volume, is effectively assigned to a unit cell in the pseudo-cubic lattice. In the effective cubic unit cell (Figure 1 b), Na cations at the A site are coordinated to twelve oxygen anions, affording $NaO_{12}$ cuboctahedra. Tantalum cations at the B site are at the center of the $TaO_6$ octahedra.

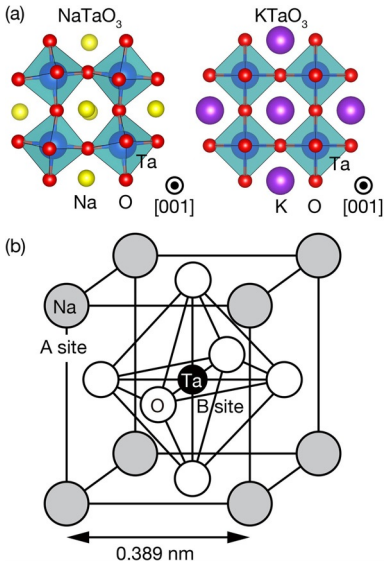


**Figure 1.** Perovskite-structured lattice of $NaTaO_3$. a) A ball-and-stick view of the lattice distorted in orthorhombic symmetry is compared with the cubic lattice of $KTaO_3$ with a tolerance factor of 1.05. b) An effective cell of the pseudo-cubic lattice.

The distorted lattice perturbs the electronic structure. The band gap of pristine $NaTaO_3$ is 4.0 eV with a light absorption edge near 300 nm.[1] Lithium tantalate ($LiTaO_3$), a sister compound with significant lattice distortion, shows a wide band gap of 4.7 eV.[16] Potassium tantalate ($KTaO_3$) composed of perfectly cubic cells ($a = 0.399$ nm),[17] presents a narrow band gap of 3.6 eV.[16] The band gaps, in the order of $LiTaO_3$ (wide) > $NaTaO_3$ > $KTaO_3$ (narrow), are related to the reduced symmetry of the original cubic lattice. In this series of tantalates, $TaO_6$ octahedra are assembled in a corner-sharing network. The cubic sublattice of Ta cations in $KTaO_3$ enables maximum overlap of the Ta 5d orbitals to form the conduction band. In the distorted lattices of $NaTaO_3$ and $LiTaO_3$ in particular, the overlaps are less complete. The energy width of the conduction band should be smaller according to the less complete overlaps with the center energy intact. The bottom of the conduction band is thus raised to widen the band gap. The water splitting rate systematically responded to the band gap (Table 2). The large splitting rate on tantalates with wide band gaps suggests that the ability of band-gap-excited electrons for water reduction determines the overall splitting rate in the absence of cocatalyst.

## 3. Electron–Hole Recombination Rate

The rate of photocatalytic reactions should be proportional to the number of excited charge carriers in a simple picture. It is hence of primary importance to identify the population of photoexcited electrons and holes that are not yet recombined. Optical absorption and photoluminescence spectroscopy are

Hiroshi Onishi is a professor of physical chemistry. He has been a fellow of The Japan Society of Vacuum and Surface Science since 2010. He received his B.S., M.S., and Ph.D. in chemistry from Tokyo University. His major research interests are in molecular science at interfaces and mechanistic aspects of catalytic reactions.

**Table 2.** The rate of overall water splitting on pristine alkali tantalates in the absence of cocatalyst.[a]

| | $H_2$ production [mmol $h^{-1}$] | $O_2$ production [mmol $h^{-1}$] | Band gap [eV] |
|---|---|---|---|
| $LiTaO_3$ | 0.43 | 0.22 | 4.7 |
| $NaTaO_3$ | 0.16 | 0.09 | 4.0 |
| $KTaO_3$ | 0.03 | 0.01 | 3.6 |

[a] Aqueous suspension of the photocatalyst (1 g) was irradiated in an inner irradiation vessel with a 400-W high pressure Hg lamp. The photocatalysts were prepared in a solid-state reaction.[16]

established methods to detect excited charge carriers. In our studies, excited electrons were quantified by infrared (IR) absorption. Figure 2a shows transient IR absorption spectra of a pristine $NaTaO_3$ photocatalyst. Photocatalyst particles were fixed on a $CaF_2$ disk, placed in a vacuum cell, and irradiated with UV light pulses.[18] Infrared light transmitting through the disk was monitored in a time-resolved manner by using a grating–monochromator-based spectrometer,[19] which was sufficiently sensitive to detect absorbance changes as small as $10^{-6}$. Band-gap excitation of the $NaTaO_3$ photocatalyst induced changes in the IR absorbance. The induced absorption monotonically increased with decreasing wavenumber from 4000 to 900 $cm^{-1}$. The monotonic spectrum suggested that band-gap-excited electrons absorbed IR light.[20] Actually, the absorption weakened when the photocatalyst was exposed to an electron-consuming species ($O_2$ gas).

Infrared absorption with similar spectra has been observed and assigned to band-gap-excited electrons for a number of metal-oxide semiconductors including $TiO_2$,[21–27] $SrTiO_3$,[28] $LaTiO_2N$,[29] $K_3Ta_3B_2O_{12}$,[30] $Bi_2WO_6$,[31] and $Ga_2O_3$.[32] For further information about the electron-induced IR absorption, several reviews are available.[33–35] The electron transition from a shallow trap state, if there is any in the band gap, to the conduction band can absorb an IR photon with the according energy. Trapped electrons may also be thermally excited to the conduction band. Electrons in the conduction band absorb IR light. The two possible transitions to present a monotonic absorption spectrum are illustrated in Figure 2c. By probing with IR light, excited electrons not yet accommodated in deep trap states were detected. This provides a good means of quantifying electrons that are active for water reduction, that is, those that are energetically close to the bottom of the conduction band. Doping with La cations caused limited modification of the spectrum. A broad absorption band at 1500–3000 $cm^{-1}$ is superposed on the monotonic shape (Figure 2b). Hence, we still ascribed the absorption to band-gap-excited electrons, although the origin of the broad band was unknown.

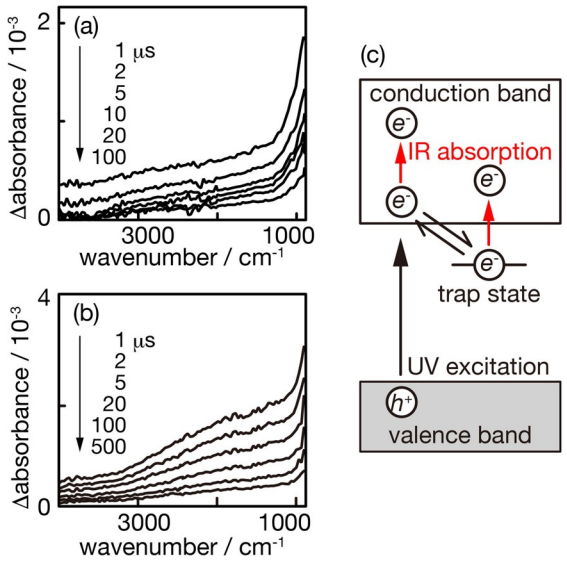


**Figure 2.** Transient IR absorption spectra of $NaTaO_3$ photocatalysts. a) A photocatalyst without doping was irradiated with pump light pulses (wavelength: 266 nm, pulse energy: 1 mJ). Absorbance change induced by the pump pulses is shown as a function of IR wavenumber and time delay. b) A photocatalyst doped with La cations (La concentration: 2 mol%) was irradiated with pump light pulses (wavelength: 266 nm, pulse energy: 0.2 mJ). c) Possible electron transitions absorbing IR photons. Reprinted with permission from ref. [18]. Copyright 2003 American Chemical Society.

Based on this assignment, transient absorbance changes provide a measure to quantify the rate of electron–hole recombination, the major path to deactivate excited charge carriers. Absorbance change should be proportional to the number of the electrons, while the absolute number cannot be determined without knowing the molar absorption coefficient of excited electrons. The recombination rate is deduced from the decay of absorbance change. Figure 3 presents absorbance change at 2000 $cm^{-1}$ as a function of time delay. Absorbance change decreased most quickly in the pristine $NaTaO_3$. Doping with La, Ca, Sr or Ba cations pushed up absorbance change in the entire range of time delay. Successful doping with these cations reduced the rate of electron–hole recombination in $NaTaO_3$ particles.

Electron decay kinetics were not simple, likely to be described with stretched exponential functions. One note about kinetics is that doping affected the recombination rate in a time-range of 1–10 μs. Decay curves of the five photocatalysts were nearly parallel at a time delay of longer than 10 μs. It was

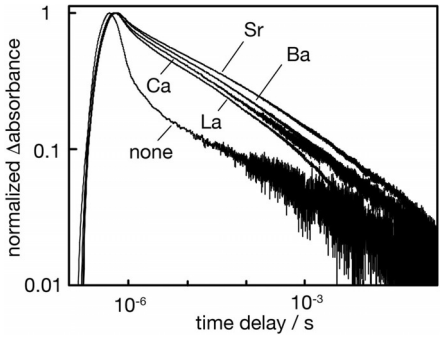


**Figure 3.** Infrared absorbance decay in $NaTaO_3$ photocatalysts doped with La, Ca, Sr, or Ba cations (doping concentration: 2 mol%) together with the decay in the pristine $NaTaO_3$ photocatalyst. Absorbance change at 2000 $cm^{-1}$ normalized at the maximum is shown as a function of time delay. Pump pulse wavelength: 266 nm. Pulse energy: 0.4 mJ. The photocatalysts were prepared by a solid-state reaction. Reprinted with permission from ref. [36]. Copyright 2009 American Chemical Society.

unfortunately difficult to reveal IR absorbance decay at 0.1 μs or shorter since our time resolution was limited by the response of IR detectors and amplifier circuits.

## 4. Steady-State Population of Band-Gap-Excited Electrons

Transient IR absorption provides a good measure of the recombination rate in $NaTaO_3$ particles. However, excitation strength in steady-state reactions is different from that employed in the transient spectroscopy. Assume a lamp produces UV light with an intensity of 1 W to irradiate a photocatalyst suspension in an inner irradiation vessel. Light flux should be 10 mW cm$^{-2}$ with an effective irradiation area of 100 cm$^2$. In transient measurements, photocatalyst particles on a disk of 1 cm$^2$ are irradiated with pump light pulses of 10 ns time width. A large light flux of 100 W cm$^{-2}$ is expected with the lowest ever reported pulse energy of 1 μJ.[18]

When we need to know the population of excited electrons available in steady-state reactions, IR absorbance changes induced by lamp irradiation should be determined. This is fortunately easy to do by using an ordinary Fourier-transform IR spectrometer. Absorbance spectra of a photocatalyst are recorded in the presence and absence of UV lamp irradiation. The absorbance change induced by UV irradiation is determined by subtracting one spectrum from the other. Figure 4 shows a set of absorbance-change spectra observed for $NaTaO_3$ photocatalysts doped with Sr cations.[37] Monotonic spectra ranging from 6000 to 900 cm$^{-1}$ appeared with a broad absorption at around 2000 cm$^{-1}$, indicating that band-gap-excited electrons produce the steady-state absorbance change.

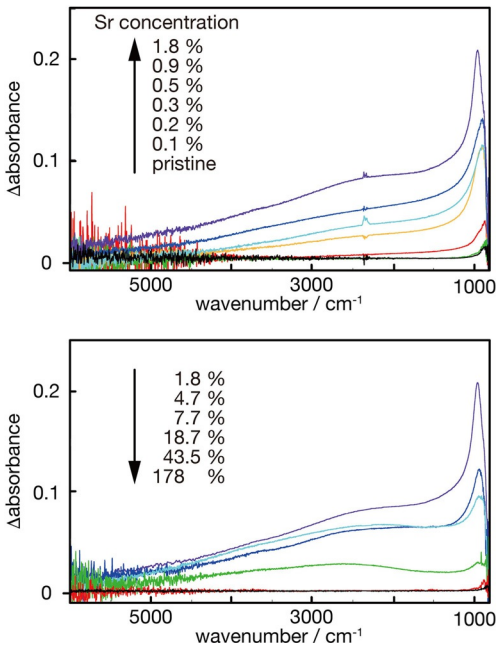


**Figure 4.** Infrared absorbance change induced by steady UV light irradiation. $NaTaO_3$ photocatalysts doped with Sr cations were irradiated with a Hg-Xe lamp (200 W). UV light flux at wavelengths of 370 nm or shorter: 60 mW cm$^{-2}$. Photocatalysts were prepared by a solid-state reaction. Reprinted with permission from ref. [37]. Copyright 2015 American Chemical Society.

The electron-induced absorption strengthened with doping concentration from zero to 1.8 mol% and weakened at higher concentrations. Doping with Sr cations increased the steady-state population of excited electrons present in the particles placed in the vacuum. The electron population was quantified by the absorbance change integrated over each spectrum. The maximum population with a dopant concentration of 1.8 mol% increased by 180 times relative to that in the pristine $NaTaO_3$ photocatalyst. Doping with Ca,[37] Ba,[37] or La[38] also increased the steady-state populations of excited electrons by 50 times or more.

We now answer our fundamental question of why quantum efficiency is increased by doping with metal cations. Successful doping restricts electron–hole recombination in $NaTaO_3$ particles and hence increases the population of excited charge carriers under UV lamp irradiation. A revised question arises; why is the recombination rate reduced by cation doping?

## 5. B-Site Substitution to Control Recombination Rates

A hint for answering the question was given in characterizing photocatalysts prepared through a hydrothermal reaction. Kudo and co-workers prepared their photocatalysts by a solid-state reaction.[1,2,10,11] Researchers including ourselves often followed their method in preparing photocatalysts with different dopants. Hydrothermal,[39] solvothermal,[40] flux,[41–44] and sol–gel[45,46] reactions were additionally examined. Hydrothermal reactions are known to yield highly cubic $NaTaO_3$ particles. An and Onishi prepared photocatalysts doped with Sr, Ca, or Ba by hydrothermal reaction and examined the steady-state population of excited electrons by using IR absorption.[37] The cubic particles that they produced exhibited negligible IR absorbance change under UV light irradiation. Metal cation doping through the hydrothermal reaction failed to reduce the recombination rate. They compared photocatalysts prepared by solid-state and hydrothermal reactions to identify the key to controlling the recombination rate. The photocatalysts prepared in the two methods presented qualitatively different Raman spectra, as shown in Figure 5. An intense band appeared at 860 cm$^{-1}$ and was strengthened by doping through the solid-state reaction. This band was totally absent with the photocatalysts doped through the hydrothermal reaction. The different Raman spectra evidenced that different compounds had been prepared. The recombination rate was reduced in the compound prepared by the solid-state reaction but was not in that prepared by the hydrothermal reaction.

Raman scattering in perovskite-structured metal oxides has been well studied. The band at 860 cm$^{-1}$ was assigned to the breathing vibration of $TaO_6$ octahedra in $NaTaO_3$. The breathing mode of vibration, which possesses $A_{1g}$ symmetry, cannot contribute to Raman scattering in a cubic perovskite-structured lattice. The selection rule of Raman scattering is governed by the symmetry of vibration mode and crystallographic lattice. The $NaTaO_3$ lattice is slightly distorted in orthorhombic symme-

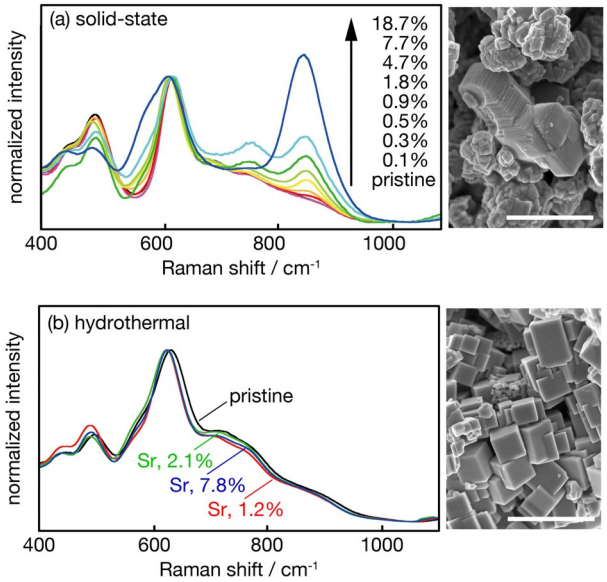


**Figure 5.** Raman spectra of $NaTaO_3$ photocatalysts doped with Sr cations through a) solid-state and b) hydrothermal reactions. Scanning electron micrographs of particles are inserted with scale bars of 1 μm. Sr concentration of the pictured photocatalysts: 0.9 (solid-state) and 2.1 mol% (hydrothermal). Reprinted with permission from ref. [37]. Copyright 2015 American Chemical Society.

try, as mentioned in section 2, but the distortion is not enough to produce a Raman band of detectable intensity. When a $Ta^{5+}$ cation is replaced by a different cation ($Sr^{2+}$ in the present case), the local cubic symmetry breaks down. The breathing vibration of $TaO_6$ octahedra is allowed in the Raman transition. Similar phenomena were observed in a number of B-site substituted perovskites, $AB_{1-x}B'_xO_3$.[47–49]

Therefore, the presence or absence of the band at 860 $cm^{-1}$ provided a sign of Sr cations occupying B sites in $NaTaO_3$. We can recognize the two photocatalysts as structural isomers with a common composition ($NaTaO_3$ doped with Sr cations) and different structures (doping sites). A finite fraction of Sr cations occupied B sites when prepared in the solid-state reaction and restricted electron–hole recombination. The same cations were selectively in the A sites following doping through the hydrothermal reaction, as evidenced by the absence of the Raman band at 860 $cm^{-1}$ (Figure 5b) and they did not affect the recombination rate. B-site substitution by Sr cations was key to controlling the recombination rate.

## 6. Solid Solutions for Accommodating Dopant Cations

Consider here the balance of cationic and anionic charges. Single substitution of $Ta^{5+}$ with $Sr^{2+}$ reduces the positive charge. One possible way to balance is creating oxygen anion vacancies in the doped $NaTaO_3$. This is not the case. Instead, simultaneous substitution of A and B sites takes place; three $Na^+$ are replaced with three $Sr^{2+}$ when one $Ta^{5+}$ is exchanged by one $Sr^{2+}$. $NaTaO_3$ should be transformed into $Sr(Sr_{1/3}Ta_{2/3})O_3$ by repeating the simultaneous substitution. Actually, $Sr(Sr_{1/3}Ta_{2/3})O_3$ has been synthesized and identified by X-ray diffraction.[50] The effective unit cell volume of $NaTaO_3$ increases from 0.236 $nm^3$ for one $NaTaO_3$ unit to 0.282 $nm^3$ per one $Sr(Sr_{1/3}Ta2_{/3})O_3$ unit.[51] Exchange of the small $Ta^{5+}$ by large $Sr^{2+}$ induces volume expansion by 19%. Exchange of $Na^+$ and $Sr^{2+}$ contributes little to the unit cell volume, since the two cations are of compatible radii.[14]

The unit cell volume of photocatalysts doped with Sr cations was determined by XRD[37] and plotted as a function of Sr/Ta molar ratio in Figure 6. A linear relation, which is predicted on the $NaTaO_3$–$Sr(Sr_{1/3}Ta_{2/3})O_3$ solid solution, fitted the determined volumes. The complete fit demonstrated evidence of the solid solution in the photocatalysts. Rietveld analysis of the X-ray diffraction data further supported the formation of the solid solution to accommodate Sr cations in $NaTaO_3$.[52]

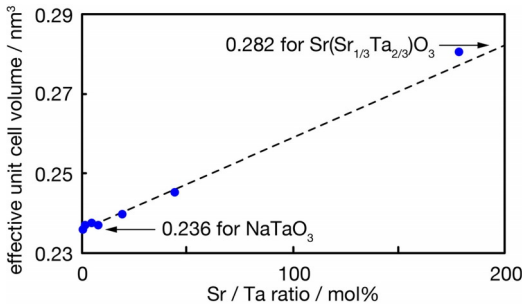


**Figure 6.** The effective unit-cell volume of solid-state-prepared $NaTaO_3$ photocatalysts doped with Sr cations. The dashed line shows the linear relation predicted in the $NaTaO_3$–$Sr(Sr_{1/3}Ta_{2/3})O_3$ solid solution. Reprinted with permission from ref. [37]. Copyright 2015 American Chemical Society.

The $NaTaO_3$–$Sr(Sr_{1/3}Ta_{2/3})O_3$ solid solution is able to accommodate $Sr^{2+}$ with no requirement for creating oxygen anion vacancies. Since cations are nearly in contact with anions in a perovskite-structured lattice, anion vacancies would decrease electrostatic energy gain. The lattice free from anion vacancy is advantageous for hole transport to increase quantum efficiency. Simultaneous doping with $La^{3+}$ and transition metal cations has been examined to sensitize $NaTaO_3$ to visible light.[38,53–56] The $NaTaO_3$–$Sr(Sr_{1/3}Ta_{2/3})O_3$ solid solution photocatalysts are recognized as $NaTaO_3$ doped with one metal element, Sr.

The local environment of Sr cations embedded in the solid-solution photocatalysts was characterized by using extended X-ray absorption fine structure (EXAFS) spectroscopy.[52] Two Sr–O shells were revealed in the solid-solution as expected. The small shell, with a short Sr–O bond length of 0.196 nm, corresponded to $SrO_6$ octahedra embedded in the corner-sharing network of $TaO_6$ octahedra. The other shell, with a Sr–O bond length of 0.260 nm, corresponded to $SrO_{12}$ cuboctahedra with Sr cations at A sites. Figure 7a shows the $k^3$-weighted X-ray absorbance spectra at the Sr K-edge and Ta $L_3$-edge for a $NaTaO_3$ photocatalyst doped with Sr cations. The Fourier transform of the Sr K-edge spectrum yielded a radial distribution function with peaks at 0.15, 0.20 and 0.31 nm (Figure 7b). The first peak, at 0.15 nm, corresponded to the Sr(B)–O shell with Sr cations at the B site. The second peak, at 0.20 nm, was related to the Sr(A)–O shell with Sr cations at the A site that Na

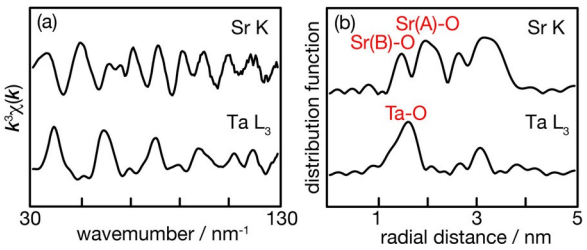


**Figure 7.** Extended X-ray absorption fine structures at the Sr K-edge and Ta $L_3$-edge observed for a $NaTaO_3$ photocatalyst doped with Sr cations through the solid-state reaction. Sr concentration: 50 mol%. a) $k^3$-weighted absorbance spectra. b) Radial distribution functions. Reprinted with permission from ref. [52]. Copyright 2018 American Chemical Society.

cations originally occupied. The radial distribution function converted from the Ta $L_3$-edge spectrum peaked at 0.16 nm.

Curve fitting was carried out to quantify the Sr–O distance in the two shells. The radial distribution functions could have been affected by the phase shifts in the electron scattering by oxygen anions. Oscillations in the $k^3$-weighted spectrum corresponding to the Sr(B)–O shell were filtered by using a window function, followed by inverse Fourier transformation to afford the shell-related oscillations. The Fourier-filtered oscillations were fitted by using one Sr–O shell with four adjustable parameters (shell length, coordination number, threshold energy difference, and squared displacement). Fitting with the Sr(A)–O shell was completed in the same manner. Table 3 summarizes the refined parameters.

**Table 3.** Metal-oxygen shells deduced from the fine structures shown in Figure 7.

| shell | $L$ [nm] | CN | d$E$ [eV] | $\sigma^2$ [pm$^2$] |
|---|---|---|---|---|
| Sr(B)–O | 0.196 | 1.1 | −0.4 | 65 |
| Sr(A)–O | 0.260 | 6.6 | −3.8 | 140 |
| Ta–O | 0.197 | 5.9 | 11.3 | 91 |

[a] $L$ = shell length; CN = coordination number; d$E$ = threshold energy difference; $\sigma^2$ = Debye–Waller factor. Reprinted with permission from ref. [52]. Copyright 2018 American Chemical Society.

The obtained Sr(B)–O bond length (0.196 nm) was compatible with the Ta–O bond length in the same photocatalyst (0.197 nm) and also with that (0.195 nm) in the effective unit cell shown in Figure 1. $SrO_6$ octahedra embedded in the solid solution were compressed in the surrounding $NaTaO_3$ lattice, when compared with $SrO_6$ octahedra in sodium chloride-structured SrO with a Sr–O bond length of 0.257 nm. The Sr(A)–O bond length (0.260 nm) slightly decreased relative to the Na–O bond length in the effective unit cell (0.275 nm).

## 7. Nanoscale Architectures for Driving Electron Excitation

Our fundamental question is now updated; how do Sr cations at B sites control recombination in the solid solution photocatalysts? The steady-state population of excited electrons gives us a suggestion. Look at Figure 4 again. The electron-induced IR absorption was strengthened by doping up to 1.8 mol% with a 180-fold enhancement. Integrated absorbance decreased beyond this concentration to a minimum at the most Sr-rich end (Sr/Ta = 187 mol%). Yoshioka et al.[50] reported that the water splitting reaction rate was low on pristine $Sr(Sr_{1/3}Ta_{2/3})O_3$, $Sr_4Ta_2O_9$ in their notation. The reduced reaction rate can be attributed to the decreased population of electrons. These results give a volcano-shaped response to doping concentration. We ask ourselves what the reason is for the volcano-shaped response. It is not obvious that Sr cations reduced the recombination rate below a threshold concentration but increased it above that threshold.

An et al.[57] proposed that the recombination rate was controlled by the concentration gradient of Sr cations at the B site in the photocatalyst particles, not by the absolute concentration of Sr cations at the B site. Their hypothesis was inspired by the volcano-shaped dependence and supported by significant Sr segregation to the particle surface, which was detected in X-ray photoelectron spectroscopy.[37] Doping with Sr cations creates graded Sr concentrations in $NaTaO_3$ particles that were originally uniform in chemical composition. The gradient should increase with Sr dosage at low dosages below a threshold. With larger Sr dosages, the concentration gradient reduces, since Sr cations are gradually distributed in the bulk. The gradient finally vanishes at the high-dosage extreme, homogeneous $Sr(Sr_{1/3}Ta_{2/3})O_3$. They chemically etched Sr-doped photocatalysts and evaluated the steady-state population of excited electrons in the etched photocatalysts. The observed response to etching time supported the hypothesis.[57]

A more recent study further evidenced the essential role of the graded composition.[58] $NaTaO_3$ photocatalysts were doped with Sr cations through crystallization in molten NaCl flux maintained at 1423 K. Chemical composition and simultaneous doping to form the $NaTaO_3$–$Sr(Sr_{1/3}Ta_{2/3})O_3$ solid solution were checked and confirmed. Immersion time in the hot flux was tuned to intentionally modify the intraparticle distribution of Sr cations with a fixed Sr concentration of 2 mol%. Curtailed immersion for 1 h produced particles capped with a 3 nm-thick Sr-accumulated layer. Figure 8 shows scanning transmission electron microscope images of the 1 h-immersed photocatalyst. A particle with a side length of 150 nm was present in the annular dark field image (Figure 8a). The upper corner of the particle is magnified in Figure 8b to show well-crystallized columns of Ta atoms. The principal elements—Ta, O, and Na—presented homogeneous distributions from the bulk to the surface in the element maps (Figure 8c). Strontium alone exhibited an accumulated layer capping the surface of the particle. The thickness of the Sr-accumulated layer was 3 nm, as deduced in the line profile (Figure 8d). Extended immersion for 60 h yielded particles with homogeneous Sr distribution.

Figure 9 shows the change in IR absorbance induced by Hg–Xe lamp irradiation. The steady-state population of excited electrons was enhanced in the 1 h-immersed photocatalyst by 160 times relative to that in a Sr-free $NaTaO_3$ photocatalyst. Doping with Sr cations in the flux increased the electron popu-

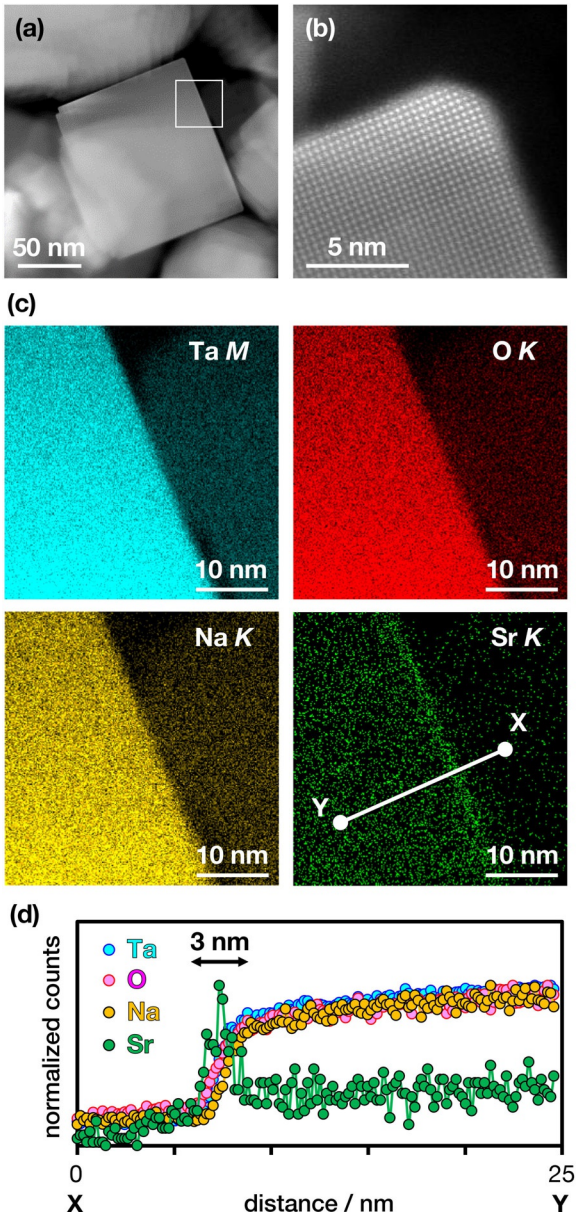


**Figure 8.** Scanning transmission electron micrographs of the photocatalyst immersed in the NaCl flux for 1 h. a) Annular dark field image. b) Ta atom columns in a particle. c) Element maps obtained with Ta M, O K, Na K, and Sr K emissions. The analyzed portion is marked with a white square in (a). d) X-ray count profiles along line *x*–*y*. Reprinted with permission from ref. [58]. Copyright 2018 American Chemical Society.

lation, which was achieved by doping through the solid-state reaction. Integrated absorbance change decreased with extended immersion time. In the 60 h-immersed photocatalyst, the population enhancement was no more than 9 times. The systematic reduction demonstrates that the excited electron population is sensitive to immersion time and thus to how Sr cations are distributed in each particle.

The thickness of the accumulated layer was 3 nm on the 1 h-immersed photocatalyst. The single-nanometer-scale architecture on 50—100 nm-sized particles enhanced the excited electron population by 160 times. This increase is reasonable since the layer thickness was compatible to the penetration

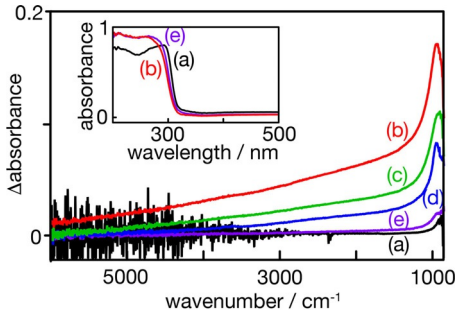


**Figure 9.** Infrared absorbance change induced by Hg–Xe lamp irradiation. a) Sr-free $NaTaO_3$; b) 1 h-, c) 10 h-, d) 20 h-, and e) 60 h-immersed $NaTaO_3$ doped with Sr cations. Strontium concentration was fixed at 2 mol%. Ultraviolet light absorption spectra of (a), (b), and (e) are shown in the inset. Reprinted with permission from ref. [58]. Copyright 2018 American Chemical Society.

depth of excitation light. With photon energies sufficiently greater than the band-gap energy of a semiconductor, the absorption coefficient increases to the order of $10^8$ $m^{-1}$.[59] The penetration depth of excitation light is hence limited to the order of 10 nm. Electrons and holes were created in or near the accumulated layer where the number of Sr cations at the B site was reduced from the surface to the bulk.

In the $NaTaO_3$–$Sr(Sr_{1/3}Ta_{2/3})O_3$ solid solution, $SrO_6$ octahedra are embedded in the network of $TaO_6$ octahedra. The embedded $SrO_6$ octahedra hinder the overlap of the Ta 5d orbitals, which narrows the conduction band with the upward shift of the band minimum. Hence, the graded concentration of the Sr cations induces the graded energy of the conduction band minimum. Band-gap-excited electrons are driven by the energy gradient to be separated from holes (Figure 10). The upward shift of the conduction band minimum was estimated to be 0.1 eV or less. Absorption edge shifts induced by doping with Sr cations were 5–10 nm according to the UV absorption spectra shown in the inset of Figure 9. An absorption edge shift by 10 nm at 300 nm corresponded to a band gap broadened by 0.1 eV.

The Sr-accumulated layer, a nanometer-scale architecture on top of the photocatalyst particles, enhanced electron–hole separation to increase the steady population of the excited charge carriers by more than two orders of magnitude. The conduc-

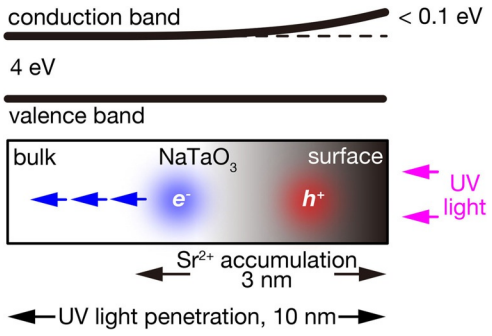


**Figure 10.** Band-gap-excited electrons driven away from holes on the energy gradient of the conduction band minimum. Reprinted with permission from ref. [58]. Copyright 2018 American Chemical Society.

tion-band structure depicted in Figure 10 resembles that of a graded junction in semiconductor devices. Doping $NaTaO_3$ with Sr cations through solid-state or flux preparation methods unintentionally created graded junctions on the particle surface where excitation light was absorbed. This scheme provides a deductive interpretation about the volcano-shaped dependence of the recombination rate.

## 8. Water Splitting Rate Compared with Photoexcited Electron Population

In the preceding sections, we asked ourselves how Sr cations control recombination in $NaTaO_3$ photocatalysts and determined that uneven Sr distributions drive excited electrons away from holes. The steady-state population of charge carriers increases according to the recombination rate. In this section, we will find a relationship between the water splitting rate and the photoexcited electron population.

The water splitting rate was examined over the four Sr-containing photocatalysts (Sr concentration = 2 mol%) prepared in the NaCl flux.[58] $H_2$ and $O_2$ production rates are plotted in Figure 11 as a function of integrated absorbance change evaluated with the spectra shown in Figure 9 (i.e., the photoexcited electron population). Two Sr-containing photocatalysts immersed in the flux for 60 and 20 h exhibited production rates nearly proportional to the integrated absorbance change, suggesting a constant efficiency of electron-to-$H_2$ and hole-to-$O_2$ conversion. The proportional relation broke down with the other two photocatalysts immersed for 10 and 1 h. These two photocatalysts with significant concentration gradients produced less $H_2$ and $O_2$ than expected on the proportional relation. Sr-accumulated layers capping the photocatalyst particles increased the charge carrier concentrations, but did not necessarily lead to higher water splitting rates. When the upward shift of the bottom of the conduction band is large enough relative to the thermal energy at RT (25 meV), only a limited fraction of electrons override the gradient to contribute to reactions at the surface. Here we learned that creating the graded composition had a dual purpose; the electron population increased and its fraction contributed to the reaction decreased.

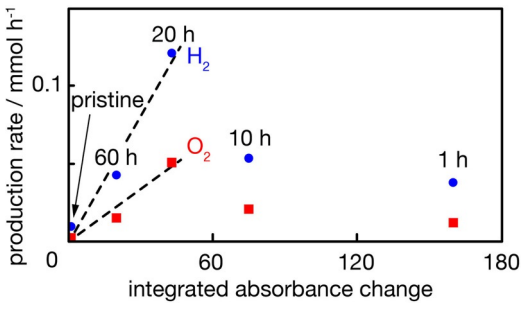


**Figure 11.** The water splitting reaction rate over the flux-prepared photocatalysts. $H_2$ (circles) and $O_2$ (squares) production rates were determined in the absence of cocatalyst and plotted as a function of integrated IR absorbance change, which was evaluated from the spectra depicted in Figure 9. The dashed lines are for eye guidance. Aqueous suspension of the photocatalysts was irradiated in an inner irradiation vessel with a 400 W high-pressure Hg lamp. Reprinted with permission from ref. [58]. Copyright 2018 American Chemical Society.

The water splitting rate was also related to the electron–hole recombination rate in the pristine and seven photocatalysts doped with Ca, Ba or La.[36] With four of the eight photocatalysts, the recombination rate was observed and already depicted as IR absorbance change in Figure 3. Absorbance change at a time delay of 10 μs relative to that at zero delay, $\Delta abs(10\ \mu s)/\Delta abs(0)$, provided a measure of the recombination rate. A large $\Delta abs(10\ \mu s)/\Delta abs(0)$ indicated slow recombination. Cation doping examined here increased $\Delta abs(10\ \mu s)/\Delta abs(0)$. The $H_2$ production rate over the four photocatalysts is plotted in Figure 12 as a function of $\Delta abs(10\ \mu s)/\Delta abs(0)$, together with the other four photocatalysts evaluated in the same manner.

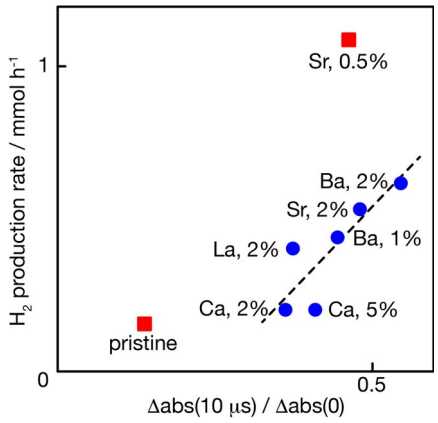


**Figure 12.** $H_2$ production rate over eight solid-state-prepared photocatalysts. $H_2$ production rate was determined in the absence of cocatalyst and plotted as a function of $\Delta abs(10\ \mu s)/\Delta abs(0)$, which was evaluated from the absorbance decay given in Figure 3. The dashed line is for eye guidance. Aqueous suspension of the photocatalysts was irradiated in an inner irradiation vessel with a 400 W high-pressure Hg lamp. Reprinted with permission from ref. [36]. Copyright 2009 American Chemical Society.

In Figure 12, six of the photocatalysts (blue circles) presented a linear relation along the dashed line, suggesting that a common fraction of excited electrons contribute to $H_2$ production. The other two photocatalysts (red squares), the pristine one and the one doped with Sr (0.5 mol%), exhibited a higher electron-to-$H_2$ conversion efficiency than the other six. Cation doping of 2–5 mol% induced surface restructuring with 10 nm-length steps and decreased the conversion efficiency simultaneously. The restructured surfaces were possibly poor catalysts for the hydrogen evolution reaction in the absence of a cocatalyst. Double edges of cation doping were again demonstrated.

## 9. Summary and Perspectives

This Minireview is devoted to the consideration of why doping with metal cations increased the quantum efficiency of water splitting reactions over $NaTaO_3$ photocatalysts. Infrared absorption of band-gap-excited photocatalysts evidenced that suc-

cessful doping reduced the electron–hole recombination rate and the steady-state population of charge carriers accordingly increased. In-depth studies using Raman spectroscopy, X-ray diffraction, extended X-ray absorption fine structure and scanning transmission electron microscopy were focused on Sr cations incorporated thorough solid-state, flux, and hydrothermal reactions. The recombination rate was found to be reduced when Ta cations in the host lattice were exchanged with Sr cations. Sodium cations were simultaneously exchanged to balance the cationic and anionic charges with no need for creating oxygen anion vacancies. $NaTaO_3$–$Sr(Sr_{1/3}Ta_{2/3})O_3$ solid solution was formed as a product of the simultaneous doping with one element. In addition to doping the proper sites, the intraparticle distribution of Sr cations played an essential role to reduce the recombination rate. Strontium cations segregated to produce graded composition from the Sr-rich surface to Sr-poor core. The bottom of the conduction band was raised at the Sr-rich surface and excited electrons were driven to the Sr-poor core, leaving holes at the surface. However, the excessively graded composition decreased the fraction of charge carriers to contribute to the surface reaction. This hypothesis has been mostly evidenced with experimental results and supplemented with a limited number of assumptions.

Charge carrier separation at step or graded junctions is widely known in semiconductor devices. The hypothesis claimed that graded junctions spontaneously appeared at the surface of $NaTaO_3$–$Sr(Sr_{1/3}Ta_{2/3})O_3$ particles and enhanced the water splitting reaction rate. The hypothesis, once received, inspired us to design graded junctions at the surface of photocatalyst particles or thin films. Actually, photoexcited electron population in $KTaO_3$ photocatalysts was enhanced by Sr doping and interpreted with similar graded junctions.[60] The thickness of surface layers to be designed is in the order of 10 nm, characterized by the light penetration depth for band-gap excitation. In addition to the hypothesized charge separation at graded junctions, surface reaction centers on $NaTaO_3$ should be investigated in coming studies.[61]

Finally, I would like to address extension to other doping elements. The studies reviewed herein were focused on doping with Sr cations. Doping with Ca or Ba cations are also effective to increase quantum efficiency (Table 1). $NaTaO_3$–$M(M_{1/3}Ta_{2/3})O_3$ solid solutions with graded distribution of M cations (M = Ca or Ba) are probably present and responsible for the increased efficiencies. The additional Raman band at 860 $cm^{-1}$ was found as expected and assigned to B-site substitution as an indicator of the increased electron population, in photocatalysts doped with Ca or Ba cations.[37] Simultaneous doping with Ca cations in $KTaO_3$ was further evidenced by X-ray fluorescence holography.[62] An interesting issue to consider is the doping sites of La cations, although simple A-site substitution is thought to occur and supported by an EXAFS study.[63] Onishi and coworkers[64] recently recognized a Raman band at 840–860 $cm^{-1}$ on solid-state-prepared photocatalysts doped with La cations. The Raman band provided a sign of the cubic symmetry locally broken down around some $TaO_6$ octahedra. It should be considered whether the locally broken symmetry does or does not suggest B-site substitution by La cations.

## Acknowledgements

*Studies reviewed herein have been conducted with a number of collaborators in different affiliations. Akira Yamakata, Toshitatsu Ikeda, Motoji Maruyama, Koji Furuhashi, Longjie An, Tomoya Fujiwara, Akira Sasahara, and Hanggara Sudrajat contributed as first authors to original papers. Mitsunori Kitta prepared the graphics shown in Figure 1 and the Table of Contents by using VESTA software.[65] Discussion with Yasuhiro Kobori and Takashi Tachikawa is acknowledged. Financial support by JSPS KAKENHI (grant numbers 21360395, 24655014, 26630411, 15H01046, 16H02250, 18F18029, and 18KK0161) is also acknowledged.*

## *Conflict of interest*

*The author declares no conflict of interest.*

**Keywords:** doping · metal oxides · photocatalysis · semiconductors · water splitting

[1] A. Kudo, H. Kato, *Chem. Phys. Lett.* **2000**, *331*, 373 – 377.
[2] H. Kato, K. Asakura, A. Kudo, *J. Am. Chem. Soc.* **2003**, *125*, 3082 – 3089.
[3] K. Teramura, S. Okubo, H. Tsuneoka, T. Shishido, T. Tanaka, *Appl. Catal. B* **2010**, *96*, 565 – 568.
[4] H. Nakanishi, K. Iizuka, T. Takayama, A. Iwase, A. Kudo, *ChemSusChem* **2017**, *10*, 112 – 118.
[5] H. Kato, A. Kudo, *Catal. Today* **2003**, *78*, 561 – 569.
[6] J. Shi, L. Guo, *Prog. Nat. Sci.* **2012**, *22*, 592 – 615.
[7] P. Kanhere, Z. Chen, *Molecules* **2014**, *19*, 19995 – 20022.
[8] T. Ahmad, U. Farooq, R. Phul, *Ind. Eng. Chem. Res.* **2018**, *57*, 18 – 41.
[9] A list of reports on perovskite-structured tantalate photocatalysts is available at http://www.edu.kobe-u.ac.jp/sci-onishi/Outcomes/natao3.html.
[10] A. Iwase, H. Kato, H. Okutomi, A. Kudo, *Chem. Lett.* **2004**, *33*, 1260 – 1261.
[11] A. Iwase, H. Kato, A. Kudo, *ChemSusChem* **2009**, *2*, 873 – 877.
[12] Y. Sakata, T. Hayashi, R. Yasunaga, N. Yanaga, H. Imamura, *Chem. Commun.* **2015**, *51*, 12935 – 12938.
[13] T. Chiang, H. Lyu, T. Hisatomi, Y. Goto, T. Takata, M. Katayama, T. Minegishi, K. Domen, *ACS Catal.* **2018**, *8*, 2782 – 2788.
[14] R. D. Shannon, *Acta Crystallogr. Sect. A* **1976**, *32*, 751 – 767.
[15] B. J. Kennedy, A. K. Prodjosantoto, C. J. Howard, *J. Phys. Condens. Matter* **1999**, *11*, 6319 – 6328.
[16] H. Kato, A. Kudo, *J. Phys. Chem. B* **2001**, *105*, 4285 – 4292.
[17] P. Vousden, *Acta Crystallogr.* **1951**, *4*, 373 – 376.
[18] A. Yamakata, T. Ishibashi, H. Kato, A. Kudo, H. Onishi, *J. Phys. Chem. B* **2003**, *107*, 14383 – 14387.
[19] K. Iwata, H. Hamaguchi, *Appl. Spectrosc.* **1990**, *44*, 1431 – 1437.
[20] J. I. Pankove, *Optical Processes in Semiconductors*, Dover, New York, **1975**.
[21] A. Yamakata, T. Ishibashi, H. Onishi, *Chem. Phys. Lett.* **2001**, *333*, 271 – 277.
[22] S. H. Szczepankiewicz, J. A. Moss, M. R. Hoffmann, *J. Phys. Chem. B* **2002**, *106*, 2922 – 2927.
[23] T. Yoshihara, R. Katoh, A. Furube, Y. Tamaki, M. Murai, K. Hara, S. Murata, H. Arakawa, M. Tachiya, *J. Phys. Chem. B* **2004**, *108*, 3817 – 3823.
[24] D. S. Warren, A. J. McQuillan, *J. Phys. Chem. B* **2004**, *108*, 19373 – 19379.
[25] D. A. Panayotov, S. P. Burrows, J. R. Morris, *J. Phys. Chem. C* **2012**, *116*, 4535 – 4544.
[26] S. Shen, X. Wang, T. Chen, F. Zhaochi, C. Li, *J. Phys. Chem. C* **2014**, *118*, 12661 – 12668.
[27] H. Sezen, M. Buchholz, A. Nefedov, C. Natzeck, S. Heissler, C. Di Valentin, C. Wöll, *Sci. Rep.* **2014**, *4*, 3808.
[28] K. Furuhashi, J. Qingxin, A. Kudo, H. Onishi, *J. Phys. Chem. C* **2013**, *117*, 19101 – 19106.

 

[29] A. Yamakata, M. Kawaguchi, N. Nishimura, T. Minegishi, J. Kubota, K. Domen, *J. Phys. Chem. C* **2014**, *118*, 23897 – 23906.
[30] T. Ikeda, S. Fujiyoshi, H. Kato, A. Kudo, H. Onishi, *J. Phys. Chem. B* **2006**, *110*, 7883 – 7886.
[31] F. Amano, A. Yamakata, K. Nogami, M. Osawa, B. Ohtani, *J. Phys. Chem. C* **2011**, *115*, 16598 – 16605.
[32] X. Wang, Q. Xu, M. Li, S. Shen, X. Wang, Y. Wang, Z. Feng, J. Shi, H. Han, C. Li, *Angew. Chem. Int. Ed.* **2012**, *51*, 13089 – 13092; *Angew. Chem.* **2012**, *124*, 13266 – 13269.
[33] A. Yamakata, T. Ishibashi, K. Takeshita, H. Onishi, *Top. Catal.* **2005**, *35*, 211 – 216.
[34] A. Yamakata, T. Ishibashi, H. Onishi, *J. Mol. Cat. A* **2003**, *199*, 85 – 94.
[35] A. Yamakata, J. J. M. Vequizo, *J. Photochem. Photobiol. C*, **2018**https://doi.org/10.1016/j.jphotochemrev.2018.12.001.
[36] M. Maruyama, A. Iwase, H. Kato, A. Kudo, H. Onishi, *J. Phys. Chem. C* **2009**, *113*, 13918 – 13923.
[37] L. An, H. Onishi, *ACS Catal.* **2015**, *5*, 3196 – 3206.
[38] H. Sudrajat, Y. Zhou, T. Sasaki, N. Ichikuni, H. Onishi, *Phys. Chem. Chem. Phys.* **2019**, *21*, 5148 – 5157.
[39] Y. Lee, T. Watanabe, T. Takata, M. Hara, M. Yoshimura, K. Domen, *Bull. Chem. Soc. Jpn.* **2007**, *80*, 423 – 428.
[40] Y. He, Y. Zhu, *Chem. Lett.* **2004**, *33*, 900 – 901.
[41] D. G. Porob, P. A. Maggard, *J. Solid State Chem.* **2006**, *179*, 1727 – 1732.
[42] S. Lee, K. Teshima, Y. Mizuno, K. Yubuta, T. Shishido, M. Endo, S. Oishi, *CrystEngComm* **2010**, *12*, 2871 – 2877.
[43] J. Sun, G. Chen, J. Pei, R. Jin, Q. Wang, X. Guang, *J. Mater. Chem.* **2012**, *22*, 5609 – 5614.
[44] A. Yamamoto, S. Mizuba, Y. Saeki, H. Yoshida, *Appl. Catal. A* **2016**, *521*, 125 – 132.
[45] C. Hu, H. Teng, *Appl. Catal. A* **2007**, *331*, 44 – 50.
[46] H. Husin, H. Chen, W. Su, C. Pan, W. Chuang, H. Sheu, B. Hwang, *Appl. Catal. B* **2011**, *102*, 343 – 351.
[47] I. G. Siny, R. Tao, R. S. Katiyar, R. Guo, A. S. Bhalla, *J. Phys. Chem. Solids* **1998**, *59*, 181 – 195.
[48] H. Zheng, I. M. Reaney, G. D. C. Csete de Györgyfalva, R. Ubic, J. Yarwood, M. P. Seabra, V. M. Ferreira, *J. Mater. Res.* **2004**, *19*, 488 – 495.
[49] G. A. Smolensky, I. G. Siny, R. V. Pisarev, E. G. Kuzminov, *Ferroelectrics* **1976**, *12*, 135 – 136.
[50] K. Yoshioka, V. Petrykin, M. Kakihana, H. Kato, A. Kudo, *J. Catal.* **2005**, *232*, 102 – 107.
[51] A cubic unit cell of $Sr(Sr_{1/3}Ta_{2/3})O_3$ with $a = 0.827$ nm contains four $Sr(Sr_{1/3}Ta_{2/3})O_3$, according to ref. [50].
[52] L. An, T. Sasaki, P. Weidler, C. Wöll, N. Ichikuni, H. Onishi, *ACS Catal.* **2018**, *8*, 880 – 885.
[53] Z. G. Yi, J. H. Ye, *Appl. Phys. Lett.* **2007**, *91*, 254108.
[54] A. Iwase, K. Saito, A. Kudo, *Bull. Chem. Soc. Jpn.* **2009**, *82*, 514 – 527.
[55] M. Yang, X. Huang, S. Yan, Z. Li, T. Yu, Z. Zou, *Mater. Chem. Phys.* **2010**, *121*, 506 – 510.
[56] P. Kanhere, J. Nisar, Y. Tang, B. Pathak, R. Ahuja, J. Zheng, Z. Chen, *J. Phys. Chem. C* **2012**, *116*, 22767 – 22773.
[57] L. An, Y. Park, Y. Sohn, H. Onishi, *J. Phys. Chem. C* **2015**, *119*, 28440 – 28447.
[58] L. An, M. Kitta, A. Iwase, A. Kudo, N. Ichikuni, H. Onishi, *ACS Catal.* **2018**, *8*, 9334 – 9341.
[59] N. S. Lewis, M. L. Rosenbluth in *Photocatalysis: Fundamentals and Applications* (Eds.: N. Serpone, E. Pelizzeti), Wiley, New York, **1989**, pp. 60 – 62 and Figure 3.8.
[60] H. Sudrajat, D. Dhakal, M. Kitta, T. Sasaki, A. Ozawa, S. Babel, T. Yoshida, N. Ichikuni, H. Onishi, unpublished results.
[61] T. Fujiwara, L. An, Y. Park, N. Happo, K. Hayashi, H. Onishi, *Thin Solid Films* **2018**, *658*, 66 – 72.
[62] A. Sasahara, T. Fujiwara, N. Happo, K. Kimura, K. Hayashi, H. Onishi, unpublished results.
[63] K. Shimura, S. Kato, T. Yoshida, H. Itoh, T. Hattori, H. Yoshida, *J. Phys. Chem. C* **2010**, *114*, 3493 – 3503.
[64] H. Sudrajat, D. Song, Y. Zhou, N. Ichikuni, H. Onishi, unpublished results.
[65] K. Momma, F. Izumi, *J. Appl. Crystallogr.* **2011**, *44*, 1272 – 1276.

Manuscript received: December 14, 2018
Revised manuscript received: February 9, 2019
Accepted manuscript online: February 15, 2019
Version of record online: March 26, 2019

 